

# **Two-Dimensional Honeycomb Monolayer of Nitrogen Group Elements and the Related Nano-Structures: A First-Principle Study**

Jason Lee<sup>1</sup>, Wen-Chuan Tian<sup>1</sup>, Wei-Liang Wang<sup>1</sup>, Dao-Xin Yao<sup>1\*</sup>

In recent years, two-dimensional materials have attracted great attention. New two-dimensional materials have been predicted, discovered, and studied. Two-dimensional materials demonstrate novel physical properties, and the study of these materials is of great importance. In this paper, we predict a new family of two-dimensional material based on the idea of octet stability: honeycomb monolayer of nitrogen group elements. From first-principle calculations, we prove the existence of two-dimensional structure of all these elements, and vibration frequencies suggest the stability of these structures. In particular, nitrogen monolayer has never been studied before. The electronic structures of these materials have also been intensively studied. The effect of spin-orbit coupling on the band structure has also been investigated. Based on analysis of projected density of states, we argue that the s and p orbitals together are sufficient to describe the electronic structure. A tight-binding model with spin-orbit coupling using only s and p orbitals that is applicable to all these materials is constructed, and the parameters are obtained by fitting the band structures to first-principle results. From these parameters, spin-orbit coupling is found to be mainly consisted of on-site term. We also study the electronic structure of both zigzag and armchair nano-ribbons, and spin-polarized ferromagnetic edge states are found in some cases. The existence of ferromagnetic edge states is in contradiction with current convention the one-dimensional systems seldom demonstrate ferromagnetism. Our study aims contribute to the study of low-dimensional materials.

---

<sup>1</sup>State Key Laboratory of Optoelectronic Materials and Technologies, School of Physics and Engineering, Sun Yat-Sen University, Guangzhou 510275, China. Correspondence and requests for materials should be addressed to D. X. Y. (email: yaodaoy@mail.sysu.edu.cn)

Low dimensional systems generally refer to systems in zero, one or two dimension. In particular, various two-dimensional (2D) materials are booming in recent years<sup>1,2</sup>. 2D materials possess novel physical and chemical properties. For example, graphene has remarkable mechanical, thermal, and electronic properties. 2D transition metal dichalcogenides have peculiar optical properties<sup>3,4</sup>. The study of 2D materials has promising future application, thus it is of great importance.

Successful exfoliation of graphene marked the beginning of study of 2D materials<sup>5,6,7</sup>. Early this year, black phosphorus was synthesized and studied<sup>8,9,10</sup>. It was argued that black phosphorus has high carrier mobility, and has certain advantage over other two-dimensional materials<sup>8</sup>. Recently, another allotrope of phosphorus called blue phosphorus has been predicted, and it has much larger band gap than black phosphorus<sup>11</sup>. Later, two additional phosphorus allotropes had been predicted by first-principle study<sup>12</sup>.

Phosphorus and nitrogen belong to the nitrogen group (VA) elements in the periodic table. Besides the study of phosphorus, 2D systems involving other VA elements are also carried out. Quantum spin hall effect is predicted to exist in honeycomb X-hydride/halide (X=N-Bi) Monolayers<sup>13</sup> and BiX/SbX (X=H, F, Cl and Br) monolayer<sup>14</sup>. The topological aspects of antimony and bismuth honeycomb monolayer are also studied, and they are found to be topological insulators<sup>15,16,17</sup>. In addition, 2D nitrogen atomic sheet has been grown epitaxially on GaAs(001) surface<sup>18</sup>.

Despite all these studies, the orbitals involved in the electronic structures near Fermi level are still not clear, thus no tight-binding model applicable to these systems has been proposed. Moreover, the studies of nitrogen and arsenic monolayers are still missing in the literature. Besides, properties of the corresponding nano-ribbons have not been investigated.

In this paper, we use first-principle calculation to explore the unknown phase of VA elements in the periodic table. Both the structures of bulk and 2D monolayers are optimized, and found that these structures are stable. The electronic structures of monolayers are intensively studied, and the evolution of band structures is clearly shown. A tight-binding Hamiltonian is constructed, and the hopping parameters are obtained by fitting to band structures from first-principle calculations. We find that the on-site contribution is the leading term in SOC. Electronic structures of both armchair and zigzag nano-ribbons for all these elements are also studied. Ferromagnetism appears in zigzag nano-ribbon of P, As and Sb, and in armchair nano-ribbon of As and Sb. Several cases of nano-ribbon, while conducting edge states appear in nitrogen and bismuth zigzag nano-ribbon. The ferromagnetic edge states may contribute to useful applications, such as spin-polarized field emission. On the other hand, the appearance of conducting edge states on nitrogen zigzag nano-ribbon is a novel and counter-intuitive phenomenon that warrants deep investigation.

## Results

### Layered Structure and Monolayers

The three-dimensional (3D) AB stacking structures and the corresponding 2D structures of VA elements are optimized by first-principle calculations. We have also calculated vibration frequencies for monolayers of all VA elements, and no imaginary frequency is found, suggesting the stability of all these structures. Their structures are similar, as shown in Figure 1, and the optimized structure parameters of nitrogen (N), phosphorus (P), arsenic (As), antimony (Sb) and bismuth (Bi) are listed in Table 1, with and without van de Waals (vdW) correction. We use  $l_{bond}$  to denote bond length, and  $l'$  to denote nearest distance between atoms in adjacent layers.  $d$  and  $\Delta z$  stand for inter-layer distance and buckling.  $a$  is lattice constant. As shown in Figure 1, each layer in these 3D layered structures, have silicene-like structures. The calculated  $a$  and  $l_{bond}$  for P are 3.32Å/3.28 Å (with/without vdW) and 2.27 Å for bulk, respectively, and 3.28 Å and 2.27 Å for monolayer, respectively, in agreement with previous study by Z. Zhu *et.al.*<sup>7</sup>. But their inter-layer distance is larger than our result.

As shown in Table 1, the  $l_{bond}$ 's are much smaller than the  $l'$ 's. The structure parameters of monolayer only slightly differ from that of the bulk. It is clear that the structure parameters for nitrogen are much smaller than that of any other VA elements. The inclusion of vdW correction mainly affects the  $d$  while having only minor effect on the  $a$ 's,  $\Delta z$ 's and  $l_{bond}$ 's. When vdW is included, all the  $l'$ 's are about twice the vdW radii. In other words, inclusion of vdW interaction does not change the structure parameters within a layer dramatically, even though there are noticeable changes in the  $d$ 's, such as for P and As. All these phenomena suggest that layers couple with each other by weak vdW interaction and thus can easily exfoliated to form monolayer<sup>19</sup>. This theoretical prediction may provide guidance to experimental synthesis and applications.

Even though there is no monotonous increase of  $d$ 's, the monotonous increases of  $a$ ,  $\Delta z$ 's,  $l_{bond}$ 's and  $l'$ 's with respect to increasing atomic number from N to Bi are clear. This is in agreement with the periodic law of elements, in that the atoms become larger with increasing atomic number. Interestingly, if we compare the bond length with twice the covalent radius, the bond length is a little bit longer.

It is necessary to point out that, during the optimization process of three-dimensional structure of N, we found the tiny jittering of total energy as the inter-layer distance changes. This may suggest that interaction between N layers are extraordinarily weak (if they have any), and the computer finds it difficult to optimize the structure to minimize the total energy. This means that these layers can detach from each other very easily, therefore the three-dimensional structure of N may not exists, and it is just a possibility.

### Electronic Structure of Monolayer

The band structures obtained from our first-principle calculation shown in Figure 2

(without SOC) and Figure 3 (with SOC), and the band gaps for all the monolayers are listed in Table 2, with and without SOC. The projected density of states (PDOS) are presented in Figure 4.

From analysis of PDOS, it is clear that the electronic structures of all the monolayers are mainly made up of s and p orbitals. N has no 2d orbital; P has 3d orbitals, but they are vacant. Therefore, in case of N and P monolayer, the contribution of d orbital to the total density of states (DOS) is exactly zero. For As, Sb and Bi, SOC in d orbitals has non-zero but only minor contribution to the total DOS. Based on this analysis, we argue that the band structures of all these monolayers can be depicted by s and p orbitals, and d orbitals are not needed. Meanwhile, the gap between the lower branch and the middle branch enlarges as atomic number increases, which is an indication of increasing relativistic effect.

From the band structures shown in Figure 2 and Figure 3, three branches of bands are evident, and they are represented by three different colors in the figures. For all the cases, and the lower branch is mainly consisted of s orbitals while the other two branches are mainly consisted of p orbitals. For N monolayer, the band structure resembles that of silicene<sup>20</sup>; PDOS shows that the lower branch and the middle branch entangled. As atomic number increases, the lower branch gradually disentangled from the middle one, becoming lower in energy, and formed a graphene-like band structure. From analysis of PDOS presented in Figure 4, the s component of the lower branch increases with decreasing p character, but the middle and upper branch takes a totally opposite trend: the p character increases as s character decreases. It can be seen from both the band structures and PDOS's, the ranges of all these three bands shrink, suggesting the weakening interaction between orbitals as the covalent bonds become longer.

As shown in Table 2, the band gap decreases from 3.70eV of nitrogen to just 0.55eV/0.42eV(without/with SOC) of Bi as atomic number increases, indicating a transition from insulator to semiconductor. This is consistent with the periodic law of element: the metal character increases as atomic number increases in VA elements. We obtained a slightly smaller band gap (1.97eV) than previous study of blue phosphorus monolayer (about 2eV)<sup>9</sup>. In absence of SOC, the Bi monolayer has direct band gap while all others have indirect band gaps. The valence band maximum (VBM) of As, Sb and Bi, and the conducting band minimum (CBM) of Bi are located in  $\Gamma$  point while others are not. When SOC is included, all band structures have indirect band gaps, and the VBM of Bi shifts away from  $\Gamma$  point. We also try applying strain to bismuth monolayer, and find that the band gap decreases with increasing strain, then it closes for approximately 5% strain, and it reopens if strain keep increasing. This is consistent with Chuang's studies that focus on the topological aspect of bismuth monolayer<sup>18</sup>; they claimed that bismuth monolayer is non-trivial 2D topological insulator.

By comparing the band structure with and without SOC, as shown in Figure 2 and

Figure 3, respectively, SOC breaks energy degeneracy of certain points in the band structures. As mentioned before, the lower branch is mainly consisted of s orbitals, while the other two branches are mainly consisted of p orbitals, thus SOC have nonzero contribution to p orbitals, but it vanishes for s orbital because the angular moment of s orbital is zero. Therefore, SOC influence the middle and upper branch of bands while having no effect on the lower branch.

### Tight-Binding Approach to Monolayer

Based on the analysis of PDOS, it is clear that a tight-binding (TB) model with just s and p orbitals is sufficient to describe the system. We could have included d orbitals to give a more accurate description, but it may not be necessary. Recently Zolymoi *et. al.* have constructed a TB model for silicane and germanane with just s and p orbital<sup>21</sup>. In view of certain similarity between the systems we study and the system in Zolymoi's paper (silicane and germanane), we can construct a similar TB model, with minor modification.

$$\mathcal{H} = \mathcal{H}_0 + \mathcal{H}_1 + \mathcal{H}_2 + \mathcal{H}_{SO}$$

$$\mathcal{H}_0 = \sum_i [\varepsilon_s a^\dagger(\mathbf{R}_i) a(\mathbf{R}_i) + \varepsilon_p \mathbf{b}^\dagger(\mathbf{R}_i) \cdot \mathbf{b}(\mathbf{R}_i)]$$

$$\mathcal{H}_1 = \sum_{\langle i,j \rangle} [h_s(i,j) + h_p(i,j) + h_{sp}(i,j) + h.c.]$$

$$\mathcal{H}_2 = \sum_{\langle\langle i,j \rangle\rangle} [h'_s(i,j) + h'_p(i,j) + h'_{sp}(i,j) + h.c.]$$

$$\begin{aligned} \mathcal{H}_{SO} = i\lambda_I \sum_{\langle\langle i,j \rangle\rangle \alpha\beta} v_{ij} \sigma_{\alpha\beta}^z \mathbf{b}_\alpha^\dagger(\mathbf{R}_i) \cdot \mathbf{b}_\beta(\mathbf{R}_j) \\ + i\lambda_R \sum_{\langle\langle i,j \rangle\rangle \alpha\beta} \mu_{ij} (\mathbf{e}_{ij} \times \boldsymbol{\sigma})^z \mathbf{b}_\alpha^\dagger(\mathbf{R}_i) \cdot \mathbf{b}_\beta(\mathbf{R}_j) + \mathcal{H}_{On-site} \end{aligned}$$

$$h_s(i,j) = \gamma_{ss} a^\dagger(\mathbf{R}_i) a(\mathbf{R}_j)$$

$$\begin{aligned} h_p(i,j) = \gamma_{pp\sigma} [\mathbf{e}_{ij} \cdot \mathbf{b}^\dagger(\mathbf{R}_i)] [\mathbf{e}_{ij} \cdot \mathbf{b}(\mathbf{R}_j)] \\ + \gamma_{pp\pi} \{ \mathbf{b}^\dagger(\mathbf{R}_i) \cdot \mathbf{b}(\mathbf{R}_j) - [\mathbf{e}_{ij} \cdot \mathbf{b}^\dagger(\mathbf{R}_i)] [\mathbf{e}_{ij} \cdot \mathbf{b}(\mathbf{R}_j)] \} \end{aligned}$$

$$h_{sp}(i,j) = \gamma_{sp} a^\dagger(\mathbf{R}_i) (\mathbf{e}_{ij} \cdot \mathbf{b}(\mathbf{R}_j))$$

$$h'_s(i,j) = \gamma'_{ss} a^\dagger(\mathbf{R}_i) a(\mathbf{R}_j)$$

$$\begin{aligned} h'_p(i,j) = \gamma'_{pp\sigma} [\mathbf{e}_{ij} \cdot \mathbf{b}^\dagger(\mathbf{R}_i)] [\mathbf{e}_{ij} \cdot \mathbf{b}(\mathbf{R}_j)] \\ + \gamma'_{pp\pi} \{ \mathbf{b}^\dagger(\mathbf{R}_i) \cdot \mathbf{b}(\mathbf{R}_j) - [\mathbf{e}_{ij} \cdot \mathbf{b}^\dagger(\mathbf{R}_i)] [\mathbf{e}_{ij} \cdot \mathbf{b}(\mathbf{R}_j)] \} \end{aligned}$$

$$h'_{sp}(i,j) = \gamma'_{sp} a^\dagger(\mathbf{R}_i) (\mathbf{e}_{ij} \cdot \mathbf{b}(\mathbf{R}_j))$$

$$\mathbf{e}_{ij} = \frac{\mathbf{R}_i - \mathbf{R}_j}{|\mathbf{R}_i - \mathbf{R}_j|}, \nu_{ij} = \frac{(\mathbf{d}_i \times \mathbf{d}_j)^z}{|\mathbf{d}_i \times \mathbf{d}_j|}$$

Here,  $a^\dagger(\mathbf{R}_i)$  and  $a(\mathbf{R}_i)$  are the creation and annihilation operators of the s electron in lattice site  $\mathbf{R}_i$ , and  $\mathbf{b}^\dagger(\mathbf{R}_i) = (b_x^\dagger(\mathbf{R}_i), b_y^\dagger(\mathbf{R}_i), b_z^\dagger(\mathbf{R}_i))$  and  $\mathbf{b}(\mathbf{R}_i) = (b_x(\mathbf{R}_i), b_y(\mathbf{R}_i), b_z(\mathbf{R}_i))$  are the creation and annihilation operators of the p electron in lattice site  $\mathbf{R}_i$ .  $\varepsilon_s$  and  $\varepsilon_p$  in  $\mathcal{H}_0$  are the onsite energies of the s and p orbital.  $\mathcal{H}_1$  contains all the nearest neighbor hoppings and  $\mathcal{H}_2$  contains all the next nearest neighbor hoppings. Both  $\mathcal{H}_1$  and  $\mathcal{H}_2$  can be divided into three parts: hopping between s orbitals ( $h_s$  and  $h'_s$ ), hopping between p orbitals ( $h_p$  and  $h'_p$ ), and hopping between s orbital and p orbital ( $h_{sp}$  and  $h'_{sp}$ ).  $\gamma_{ss}$ ,  $\gamma'_{ss}$ ,  $\gamma_{pp\sigma}$  and so on are the corresponding hopping integrals. The first term in  $\mathcal{H}_{SO}$  is intrinsic SOC and the second term is Rashba SOC<sup>22</sup>.  $\alpha$  and  $\beta$  in  $\mathcal{H}_{SO}$  are spin indexes.  $(\mathbf{d}_i \times \mathbf{d}_j)^z$  is the z component of  $\mathbf{d}_i \times \mathbf{d}_j$ .  $\mu_{ij} = \pm 1$  for A(B) sites.  $\mathbf{d}_i$  and  $\mathbf{d}_j$  are the two nearest bonds connecting the next nearest neighbors.  $\mathcal{H}_{On-site}$  is the on-site spin-orbit coupling that comes from the fact that  $\mathbf{S} \cdot \mathbf{L}$  does not commute with  $\mathcal{H}$ . The non-zero matrix elements between different orbitals and spin components are:

		spin-up			spin-down		
		$p_x$	$p_y$	$p_z$	$p_x$	$p_y$	$p_z$
spin-up	$p_x$		$i\lambda_{OS}$				$-\lambda_{OS}$
	$p_y$	$-i\lambda_{OS}$					$i\lambda_{OS}$
	$p_z$				$\lambda_{OS}$	$-i\lambda_{OS}$	
spin-down	$p_x$			$\lambda_{OS}$		$-i\lambda_{OS}$	
	$p_y$			$i\lambda_{OS}$	$i\lambda_{OS}$		
	$p_z$	$-\lambda_{OS}$	$-i\lambda_{OS}$				

All together there are 13 parameters in this TB Hamiltonian, including three parameters of SOC. We have obtained these parameters by fitting TB band structure to the result from first-principle calculation, as presented in Table 3. The comparison between first-principle band structures and TB band structures are shown in Figure 5 (without SOC) and Figure 6 (with SOC). As can be seen from Table 3, these parameters demonstrate a clear trend that obeys the periodic law of element, with certain abnormality.  $\gamma_{sp}$  and  $\gamma_{pp\sigma}$  are dominant over all other parameters because of better overlap between orbitals. The hoppings between nearest neighbors are greater than those between next nearest neighbors. Since the SOC in N monolayer is negligibly small, the inclusion of SOC have no detectable effect on the band structure, as can be seen from first-principle results. Therefore SOC is not included in TB model of N monolayer. The contributions of three types of SOC are varied, and on-site SOC plays a more important role than the other two. On-site SOC parameters with increasing atomic number which is consistent

with our first-principle calculations. On-site SOC preserves time-reversal invariant, and may play an important role in time-reversal-invariant topological superconductors<sup>23</sup>.

### **Zigzag and Armchair Nano-ribbon**

We have calculated zigzag nano-ribbon (ZNR) and armchair nano-ribbon (ANR) with various widths. Figure 7 (a) shows a particular case of ZNR and ANR of 20 atoms wide. Before calculation of the electronic structure, the outermost three atoms on each side are fully relaxed. As shown in Figure 7 (b) to (f), the edges of nitrogen and bismuth ZNR, and the edges of nitrogen, phosphorus and bismuth ANR are found to be rearranged, while for other cases only minute atom displacements are observed. The nitrogen atoms on the edge of nitrogen ZNR and ANR moves towards the central plane (Figure 7 (b) and (d)). The edges of bismuth ZNR are obviously bent (Figure 7 (c)). The outermost bond of phosphorus and bismuth ANR are rotated, making the buckling on the edges larger than that in the center of ANR (Figure 7 (e) and (f)). There is even possible reconstruction of bismuth ANR on the edges in such a way that each atom is bonded to three neighboring ones.

Compared with the band structure of monolayer, the correspondence of the branches of bands are obvious. A particular example of phosphorus is shown in Figure 8. The lower branch of ZNR and ANR mimics the counterpart of graphene. Any bands of ZNR and ANR that have this correspondence can be obtained by projection. And the two-dimensional band gap is 2.05eV for phosphorus ZNR, slightly larger than that of the monolayer, while the “bulk” band gap for phosphorus ANR is the same as that of the monolayer.

It is interesting to notice that there are two bands of phosphorus monolayer that do not correspond to any of the bands in the monolayer. The two bands in ZNR are doubly degenerate in energy and spin, but their spins are opposite to each other. There is a gap between these two bands, which is about 0.28eV, and the Fermi level lies inside the gap. In other words, this system is ferromagnetic, and demonstrates a magnetic moment about  $2.02\mu_B$ . This is reasonable, because the band below Fermi level is doubly degenerate, and contains two electrons from each unit cell. We believe that each band corresponds to two electrons on two edges, and the magnetism comes from the overlap between wave functions on two edges. This differs from the antiferromagnetic edge state of graphene ZNR<sup>24,25</sup>. On the other hand, the two bands in ANR are four-fold degenerate, but are not spin-polarized. In other words, the edges of ANR of phosphorus are anti-ferromagnetic, processing a zero magnetic moment. We also calculate the band structures of phosphorus ZNR and ANR that are passivated by hydrogen, and the edge states disappear. Therefore it is possible that dangling bonds are responsible for edge states.

Similar band structures can be obtained for other cases, as shown in Figure 9. Strangely enough, the edge states of N and Bi ZNR, and the edge states of N and P ANR are not spin-polarized. And there seems to be no edge states for Bi ANR. Interestingly, the edge

states of N ZNR are conducting, which is in great contrast with our common sense that most materials containing nitrogen are unlikely to be conductors. The total magnetic moments per unit cell are  $2.02\mu_B$ ,  $2.00\mu_B$  and  $2.04\mu_B$  for phosphorus, arsenic, and antimony ZNR with 20 atoms wide, respectively, and  $4.05\mu_B$  and  $3.95\mu_B$  for arsenic and antimony ANR with 20 atoms wide, respectively. And there is no magnetic moment for nitrogen and bismuth ZNR, or nitrogen, phosphorus and bismuth ANR, because their edge states are not spin-polarized. We have also tried various widths, such as 22, 24, 26, 28 and 30 atoms wide, and the band structures are very similar, and the edge states are not sensitive to the width of ZNR; this may be another indication that the edge states come from dangling bonds.

Analysis of charge density reveals the existence of edge states. We found that the charge of this band is mainly distributed on both of the edges of the ZNR. Figure 10 shows the charge distribution of edge states of phosphorus ZNR with 20 atoms wide. The charge distribution for other element with various width are very similar, and are not presented here. Interestingly, for bismuth ANR, there seems to be no edge states because of possible reconstruction in which no dangling bonds exists that may contribute to edge states.

The spin-polarized edge state of ZNR can be useful in several applications. It can be used in spin-polarized angular-resolved photoemission spectroscopy (ARPES), a necessary technique in the study of topological insulator. It can also be used in spin-polarized scanning tunneling microscopy (SP-STM) as a tool to detect the spin texture of material surfaces. Likewise, spin-polarized field emission can take advantage of this polarized spin as well. The graphene ZNR may not be useful in all these cases, since the edge state of graphene ZNR is not spin-polarized, as mentioned above.

## Discussion

Using first-principle calculation, we demonstrate the existence of two-dimensional honeycomb monolayer of VA elements, and the corresponding structure parameter is given. From the three-dimensional structure, it is clear that the systems have AB stacking layered structure (with some uncertainty about N), and each layer is similar to silicene. The geometry of monolayer is very similar to that of the bulk, indicating that layers are bound together by weak van de Waals interaction. Bond length, lattice constant and buckling increase monotonously as atomic number increases from nitrogen to bismuth, obeying the periodic law of elements.

Electronic structure shows a clear trend that obeys the periodic law of elements, as atomic number goes from nitrogen to bismuth. Three branches of bands are obvious in the band structure, and they are similar for all VA elements with minor variations. Spin-orbit coupling (SOC) plays certain role in the band structures, and its effect becomes greater as atomic number increases, but its influence is still limited. SOC influences p orbitals, which can be seen from minor changes of bands that have much p characters. There is no noticeable effect of SOC on s orbitals. The band gap decreases

monotonously, from 3.7eV for nitrogen to only 0.55eV (without SOC)/0.43eV(with SOC), which means it goes from insulator to semiconductor.

From projected density of states, it is clear the s and p character of bands changes monotonously. When the atomic number is small, s and p orbitals are mixed, such as for cases of nitrogen and phosphorus. As the atomic number increases, the s character shifts downwards in energy, and becomes the dominant component of lower branch of bands; on the other hand, the p character shifts upwards in energy, becoming the dominant component of the middle branch and upper branch of bands. In all these cases, the effect of d orbital in the making of band structure is negligible. Based on this analysis, we have constructed a tight-binding (TB) Hamiltonian using only one s orbital and three p orbitals from each atom in the unit cell, and the hopping parameters are obtained by fitting the band structures. SOC is also included in this TB Hamiltonian.

Lastly, the atomic and electronic structure of zigzag nano-ribbon (ZNR) and armchair nano-ribbon (ANR) have also been studied. Rearrangements in nitrogen and bismuth ZNR and nitrogen, phosphorus and bismuth ANR are found, and there is possible reconstruction in bismuth ANR. In the study of electronic structure, we found an obvious correspondence of band structure to that of monolayer. Band structures of ZNR and ANR show spin-polarized ferromagnetic edge states for phosphorus, arsenic and antimony ZNR and arsenic and antimony ANR. The conducting edge states of nitrogen ZNR is also worthy of mentioning, since it contradicts our convention that substances made from nitrogen are usually insulators.

All these findings may contribute to the study of future use of these materials. In particular, the spin-polarized edge state may be useful in spin-polarized angular-resolved photoemission spectroscopy (ARPES), Spin-polarized scanning tunneling microscopy (SP-STM) and spin-polarized field emission.

## Methods

In this paper, we use first-principle calculation to explore the unknown phase of VA elements in the periodic table. Our calculation is based on Plane Augmented Wave (PAW) with Perdew-Burke-Ernzerh (PBE) of exchange-correlation<sup>26</sup> as implemented in the Vienna *Ab initio* Simulation Package (VASP) code<sup>27</sup>. To ensure reliable result, we use large energy cut-off of 400eV for bulk and monolayer, but we use default cut-off energy for nano-ribbon. The systems are restricted to periodic boundary conditions. A vacuum at least 15 Å thick is inserted to eliminate the interaction between different units in the study of system with low dimension (monolayer and nano-ribbon). For optimization, ions are relaxed using conjugate-gradient algorithm until the total force is no greater than 0.01eV/Å. Grimme's scheme for van de Waals (vdW) correction<sup>28</sup> is used for optimization of bulk structure, and results are compared with those obtained without vdW correction. Unfortunately, vdW correction is not included in case of bismuth because of lack of parameters. We believe that vdW has no substantial effect on the layer structure of bismuth monolayer. Some vdW scheme with higher precision<sup>29</sup> could have been used, but getting accurate vdW energy is not the main interest

of this paper, and a simple time-saving scheme of Grimme is sufficient to prove our statements. Spin-orbit Coupling (SOC) is included only in the calculation of band structure of monolayer.

## **Acknowledgments**

This project is supported by National Basic Research Program of China (2012CB821400), NSFC-11074310, NSFC-11275279, Specialized Research Fund for the Doctoral Program of Higher Education (20110171110026), and NCET-11-0547.

## **Author contributions**

J. L. took charge of all the first-principle calculations and analysis of these calculations. J. L. and W. C. T. proposed the tight-binding Hamiltonian, and all the parameters in this Hamiltonian are fitted to first-principle results by W. C. T.. W. L. W. was in charge of commercial software usage. D. X. Y. was the leader of this study. All authors participated in the writing, examination and revision of this paper.

Element		N	P	As	Sb	Bi
Bulk (without vdW)	$a$	2.29	3.28	3.62	4.21	4.46
	$\Delta z$	0.70	1.24	1.40	1.62	1.71
	$d$	3.11	4.10	3.96	2.85	2.71
	$l'$	3.38	4.52	4.47	3.75	3.74
	$l_{bond}$	1.50	2.27	2.51	2.92	3.09
Bulk (with vdW)	$a$	2.29	3.32	3.65	4.11	-
	$\Delta z$	0.70	1.21	1.37	1.64	-
	$d$	2.76	2.88	2.82	2.84	-
	$l'$	3.06	3.46	3.52	3.70	-
	$l_{bond}$	1.50	2.27	2.51	2.89	-
Monolayer	$a$	2.30	3.28	3.61	4.12	4.33
	$\Delta z$	0.70	1.24	1.40	1.65	1.71
	$l_{bond}$	1.50	2.26	2.51	2.89	3.09
Covalent radius <sup>30</sup>		0.71	1.07	1.19	1.39	1.48
vdW radius <sup>21</sup>		1.55	1.80	1.85	2.06	2.07
Unit in Å						

Element		N	P	As	Sb	Bi
Without SOC	Band gap/eV	3.70	1.97	1.59	1.26	0.55
	Gap type	Indirect	Indirect	Indirect	Indirect	Direct
	VBM	Not $\Gamma$	Not $\Gamma$	$\Gamma$	$\Gamma$	$\Gamma$
	CBM	Not $\Gamma$	Not $\Gamma$	Not $\Gamma$	Not $\Gamma$	$\Gamma$
With SOC	Band gap/eV	3.70	1.97	1.81	1.00	0.43
	Gap type	Indirect	Indirect	Indirect	Indirect	Indirect
	VBM	Not $\Gamma$	Not $\Gamma$	$\Gamma$	$\Gamma$	Not $\Gamma$
	CBM	Not $\Gamma$	Not $\Gamma$	Not $\Gamma$	Not $\Gamma$	$\Gamma$
Change of band gap duo to SOC/eV		0.00	0.01	0.21	-0.26	-0.12

Table 3 Tight-Binding Parameters for Monolayer of VA Elements (eV)

Element	N	P		As		Sb		Bi	
		No SOC	SOC	No SOC	SOC	No SOC	SOC	No SOC	SOC
$\epsilon_s$	-6.80	-5.02	-5.02	-4.90	-7.53	-5.49	-6.79	-7.09	-8.89
$\epsilon_p$	-1.67	-0.565	-0.565	-0.275	-0.452	-0.252	-0.613	-0.105	-0.563
$\gamma_{ss}$	-1.49	-1.07	-1.08	-0.351	-1.22	-0.448	-0.985	-0.0515	-0.864
$\gamma_{sp}$	4.76	2.89	2.89	1.98	2.72	1.85	2.20	1.61	1.99
$\gamma_{pp\sigma}$	-5.94	-3.34	-3.34	-2.91	-2.77	-2.29	-2.26	-2.04	-2.02
$\gamma_{pp\pi}$	1.56	0.767	0.767	0.684	0.606	0.557	0.472	0.394	0.395
$\gamma'_{ss}$	0.216	0.260	0.261	0.0986	-0.0529	0.0490	-0.0735	-0.0186	-0.124
$\gamma'_{sp}$	-0.0235	-0.0562	-0.0562	-0.0637	0.179	-0.0384	0.0280	-0.0200	-0.124
$\gamma'_{pp\sigma}$	1.38	1.15	1.15	0.858	0.786	0.653	0.646	0.535	0.551
$\gamma'_{pp\pi}$	-0.499	-0.377	-0.377	-0.233	-0.174	-0.162	-0.130	-0.109	-0.140
$\lambda_l/10^{-3}$	—	—	-0.141	—	0	—	1.97	—	0
$\lambda_R/10^{-2}$	—	—	0.406	—	0	—	0.278	—	0
$\lambda_{OS}$	—	—	-0.0106	—	-0.285	—	-0.299	—	-0.630

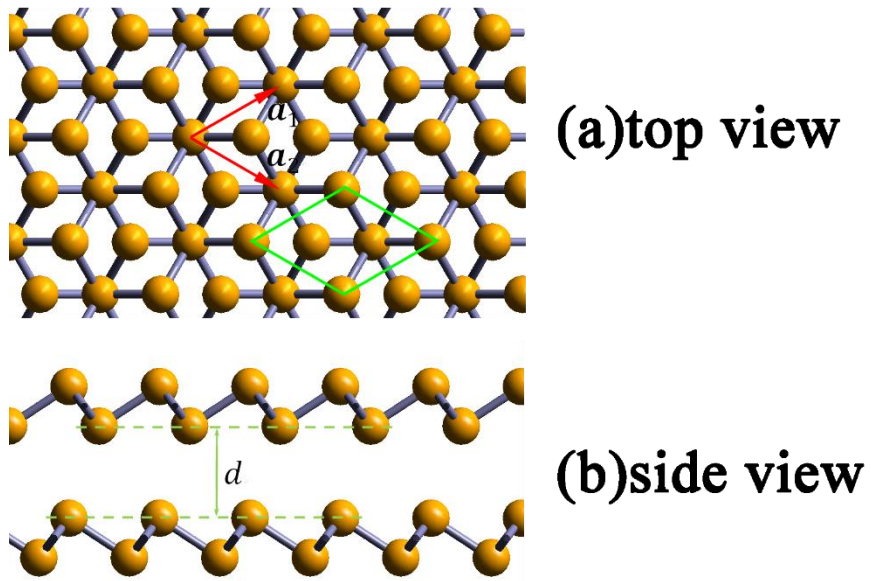


Figure 1 (a)The top view and (b) the side view of three-dimensional structure of VA elements. Red arrows are the lattice vectors in the plane. Green rhombus is the unit cell.  $d$  is the inter-layer distance.

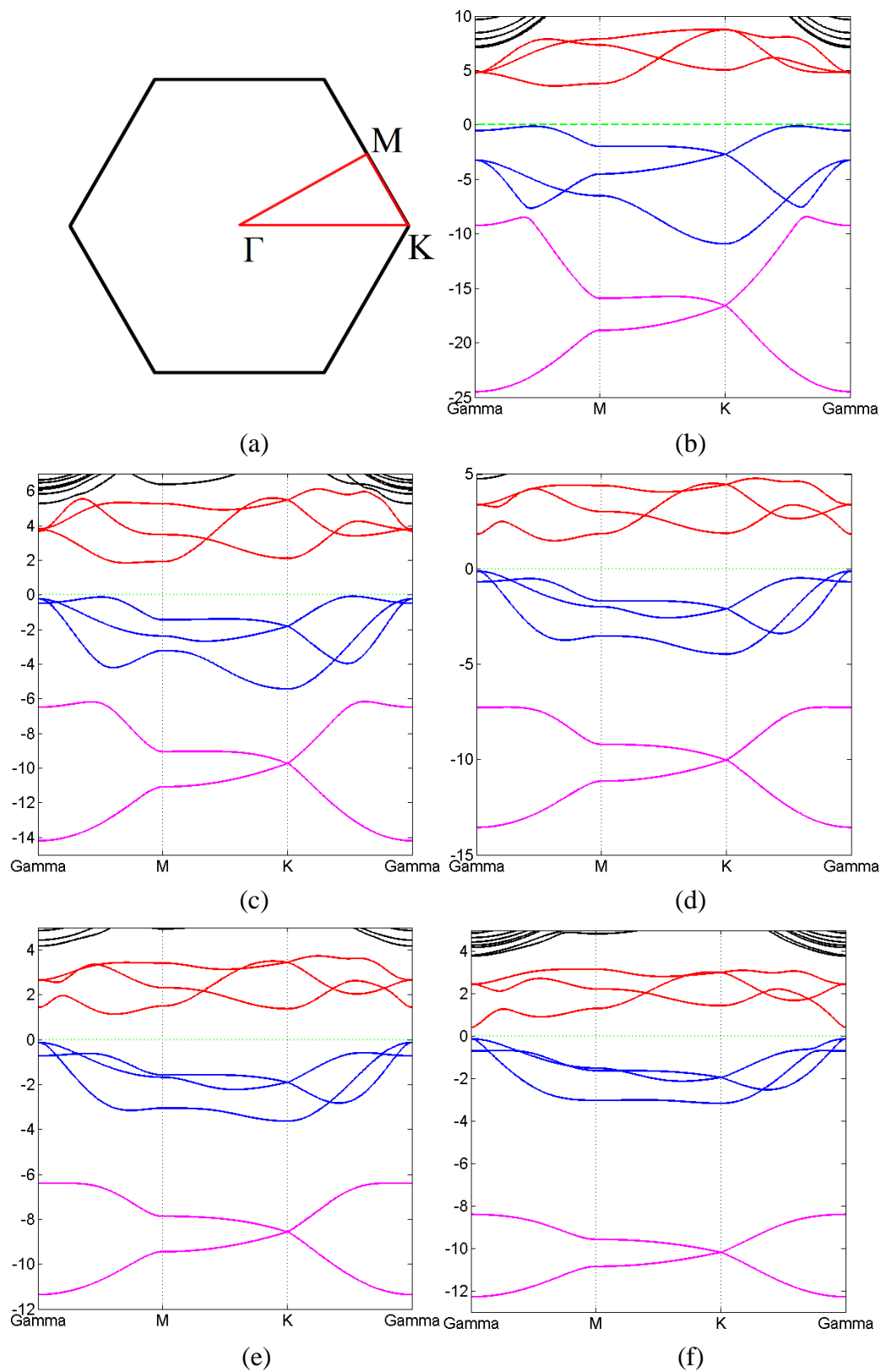
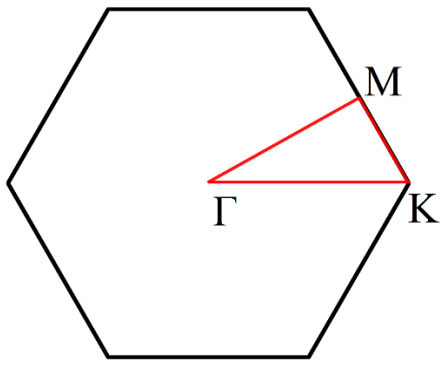
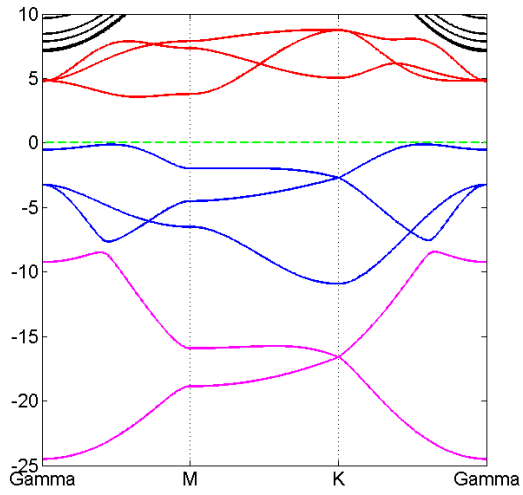


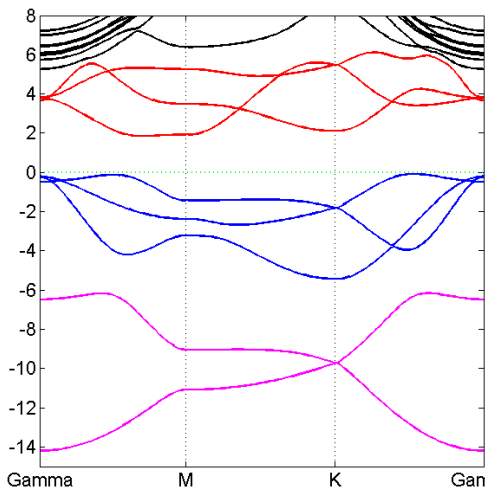
Figure 2 (a) The first Brillouin Zone and the high symmetric points of two-dimensional honeycomb lattice. (b)-(f) Band structure evolution of 2D monolayer of VA elements as it goes from nitrogen to bismuth. Different colors refer to different branches of bands. Fermi energy is set to zero denoted by green dash line.



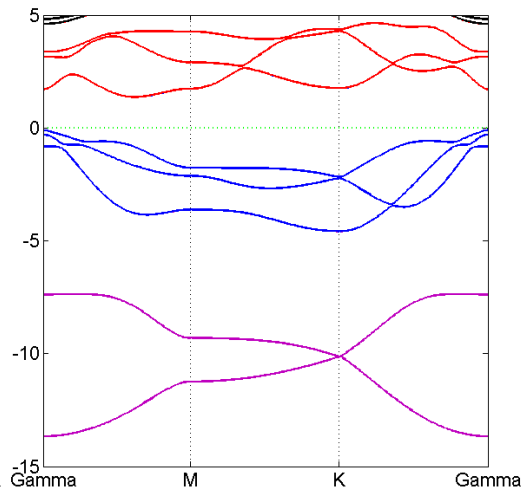
(a)



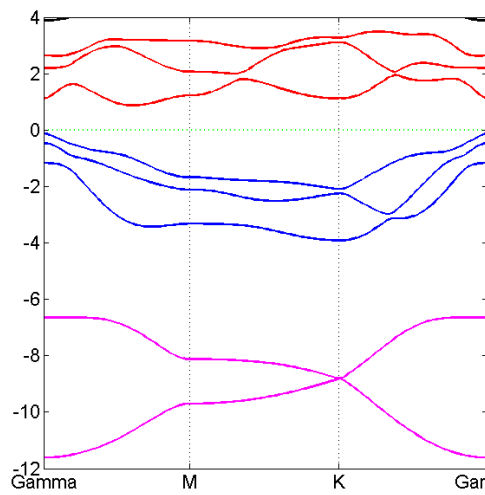
(b)



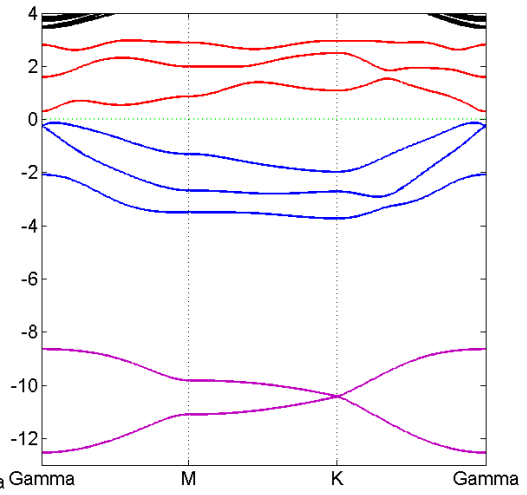
(c)



(d)



(e)



(f)

Figure 3 The same as Figure 2, but with SOC.

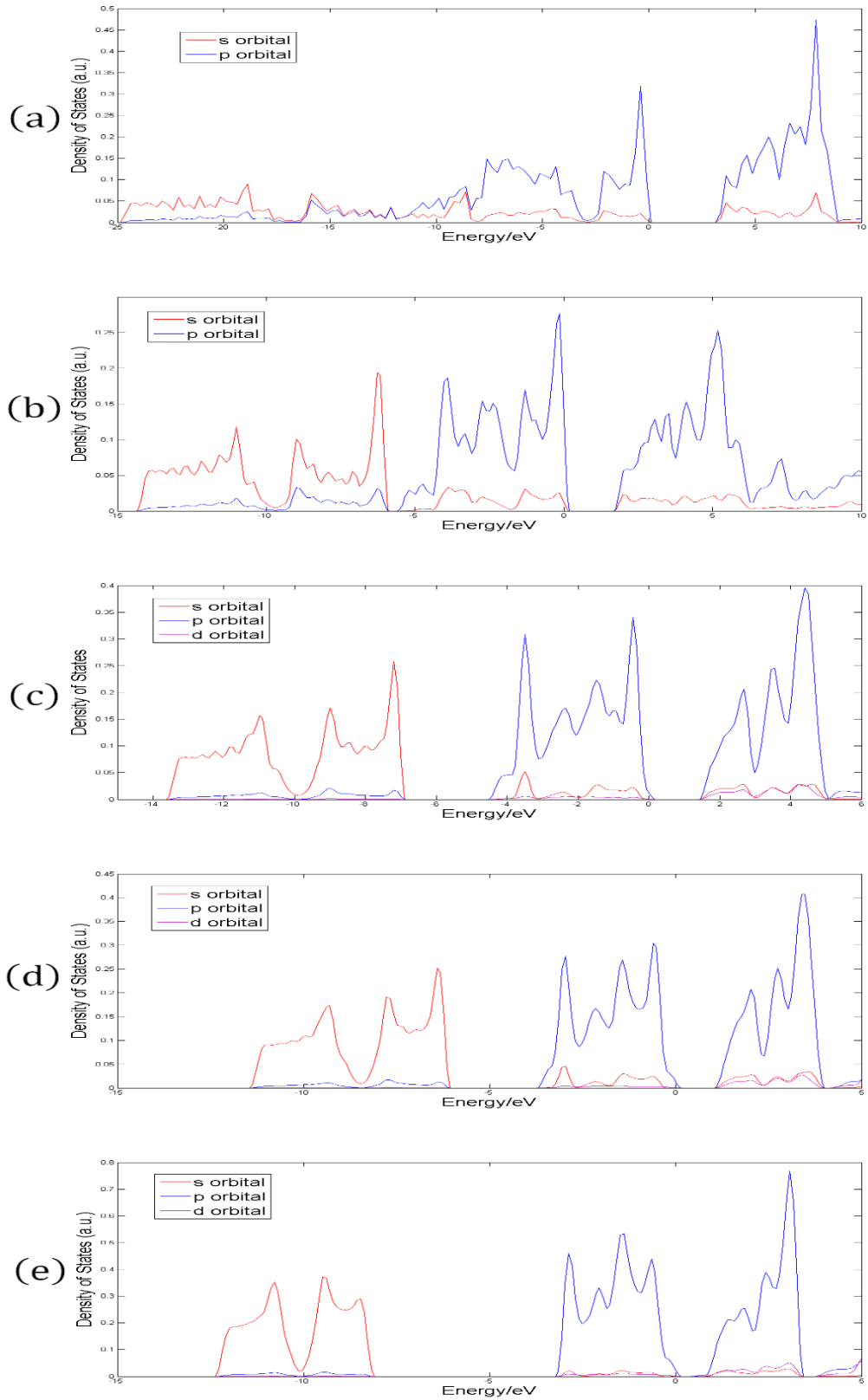
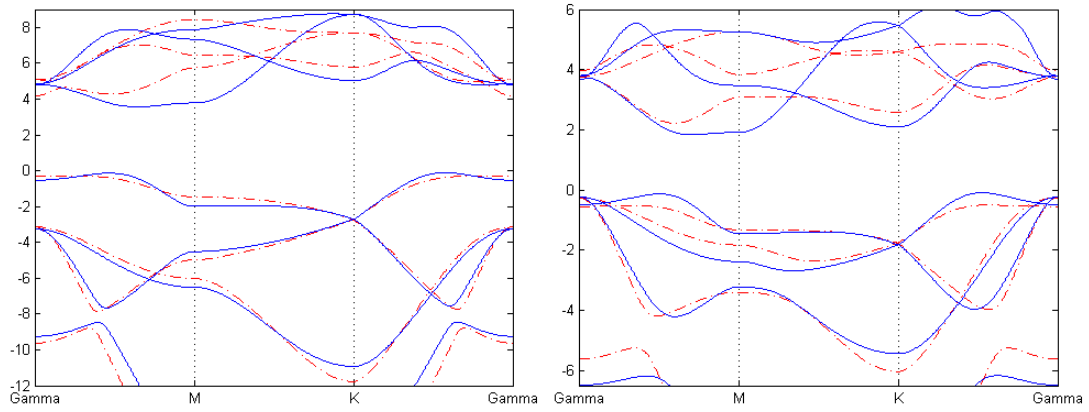
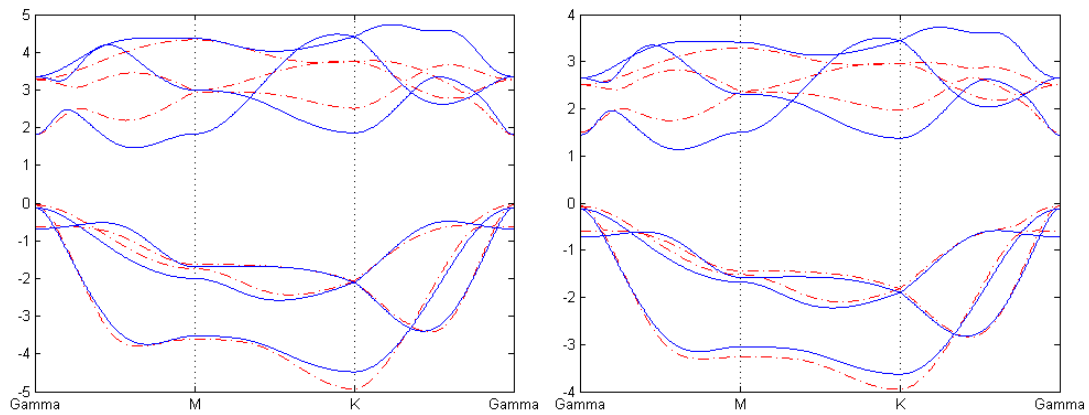


Figure 4 The density of states of monolayers of (a) nitrogen, (b) phosphorus, (c) arsenic, (d) antimony and (e) bismuth. Red, blue and purple solid lines denote the projection into s orbital, p orbital and d orbital, respectively. Fermi energy is set to zero.



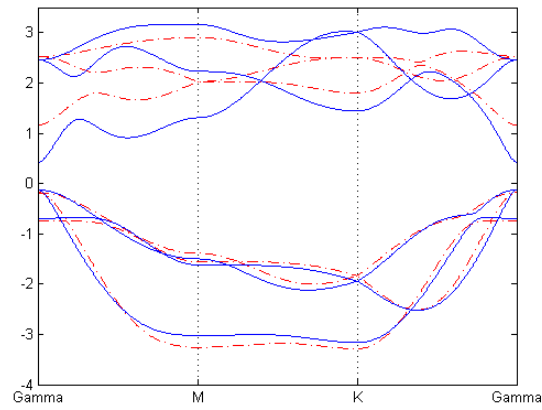
(a)

(b)



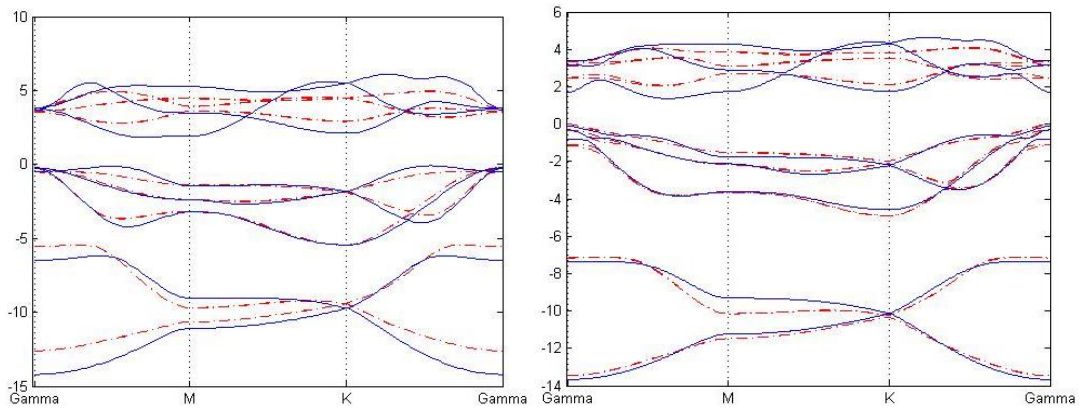
(c)

(d)



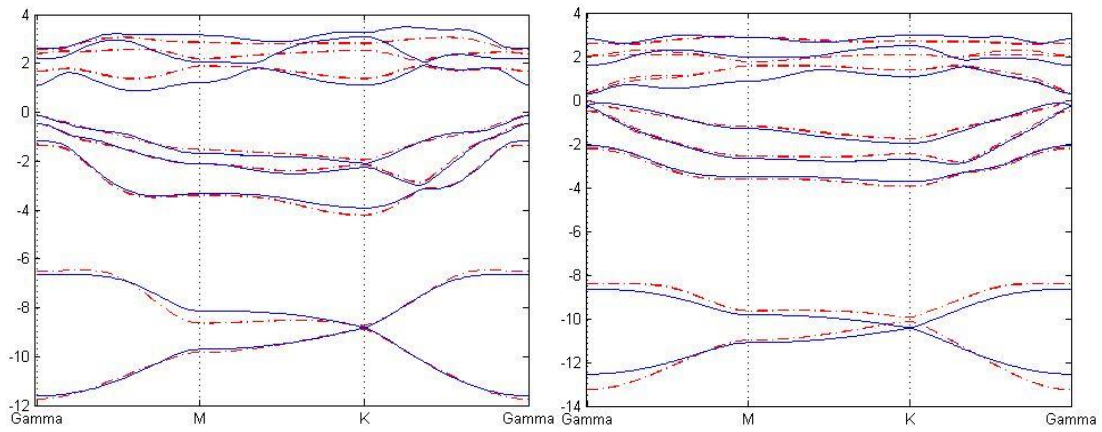
(e)

Figure 5 (a)-(e) Tight-binding band structures of 2D monolayer of VA elements as it goes from nitrogen to bismuth (red dotted line), compared with first principal results (blue solid line). The first Brillouin Zone and the high symmetric points are the same as two previous figures.



(a)

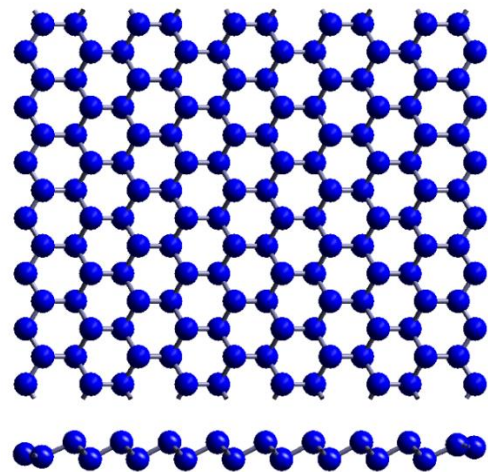
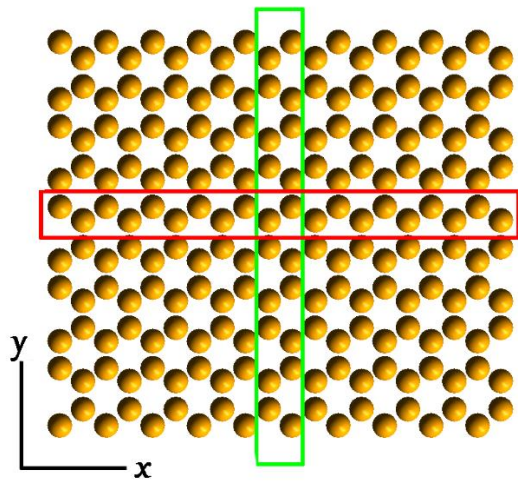
(b)



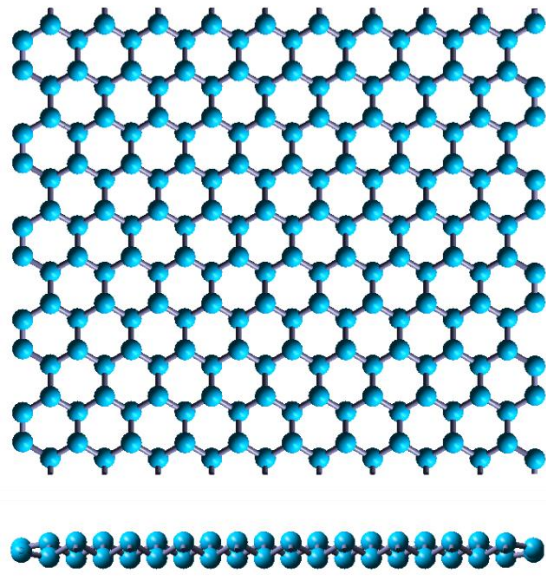
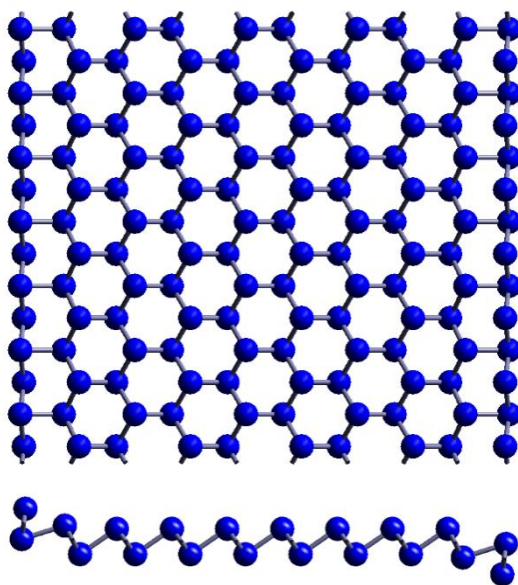
(c)

(d)

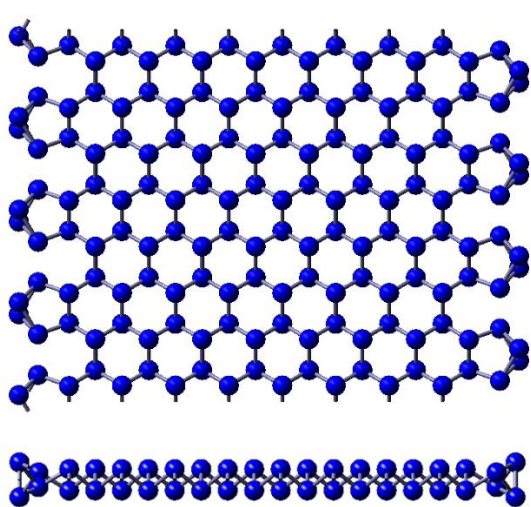
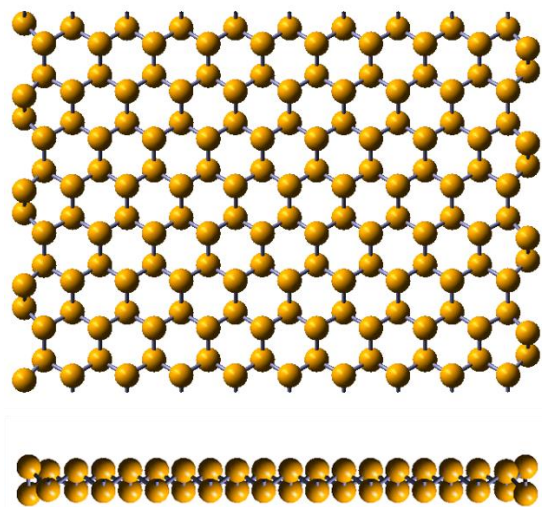
Figure 6 (a)-(d) Tight-binding band structures of 2D monolayer of VA elements as it goes from phosphorus to bismuth (red dotted line). All others are the same as Figure 5, but with SOC.



(a) (b)



(c) (d)



(e) (f)

Figure 7(a) Schematic drawing of ZNR and ANR with 20 atoms wide. The system is periodic in x direction for ZNR while it is periodic in y direction for ANR. The green and red rectangles represent the atoms in the unit cell for ZNR and ANR, respectively. Vacua of 15 Å are inserted on both sides of the nano-ribbon. (b) and (c) are the optimized structure of ZNR for Nitrogen and Bismuth, respectively. (d), (e) and (f) are the optimized structure of ANR Nitrogen and Bismuth, respectively.

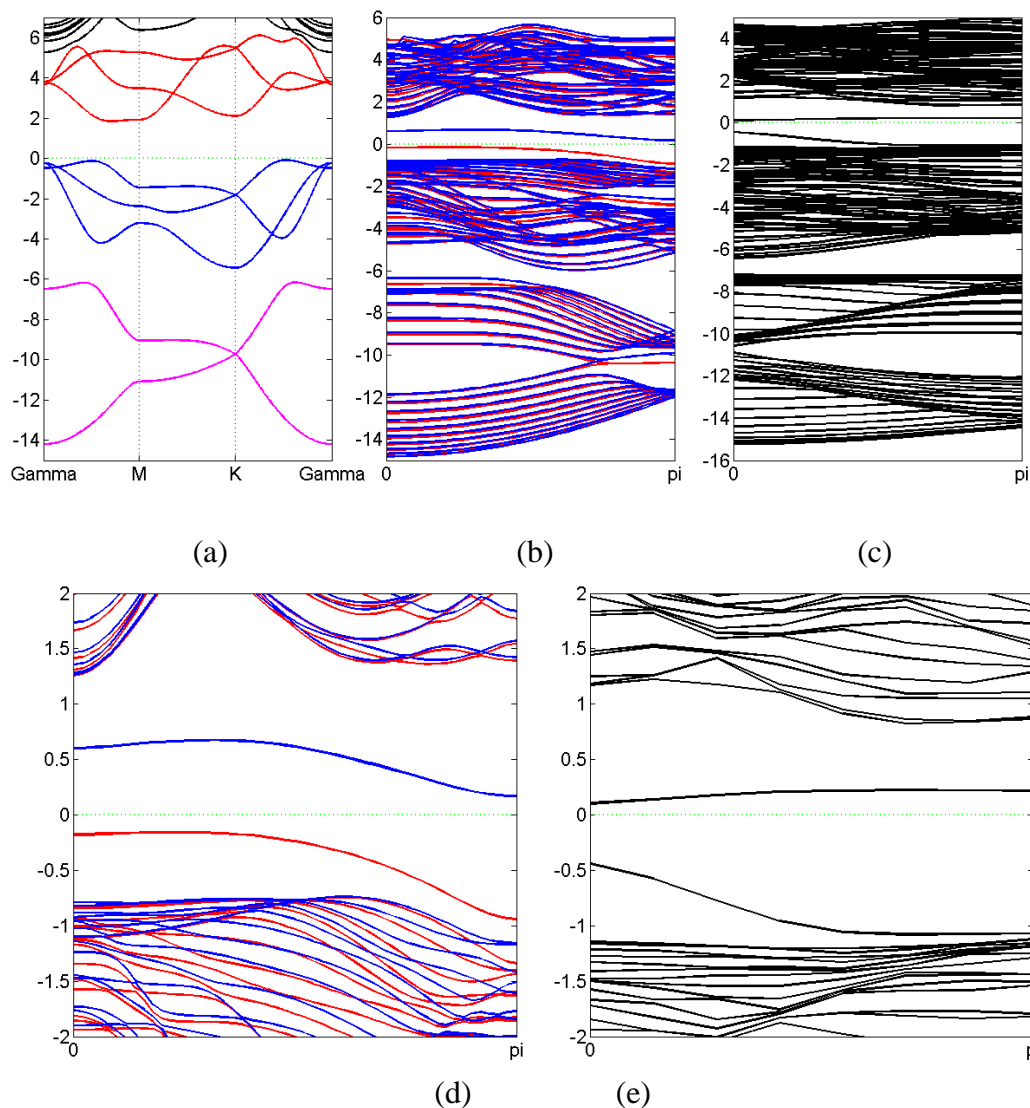


Figure 8 Band structure of zigzag blue phosphorus ZNR (b) and ANR (c) compared with that of monolayer (a). (d) and (e) Same as (b) and (c), but the energy scale is different. The Fermi level is denoted by green dash line. Red and blue solid lines in (b) and (d) refer to spin-up and spin-down, respectively.

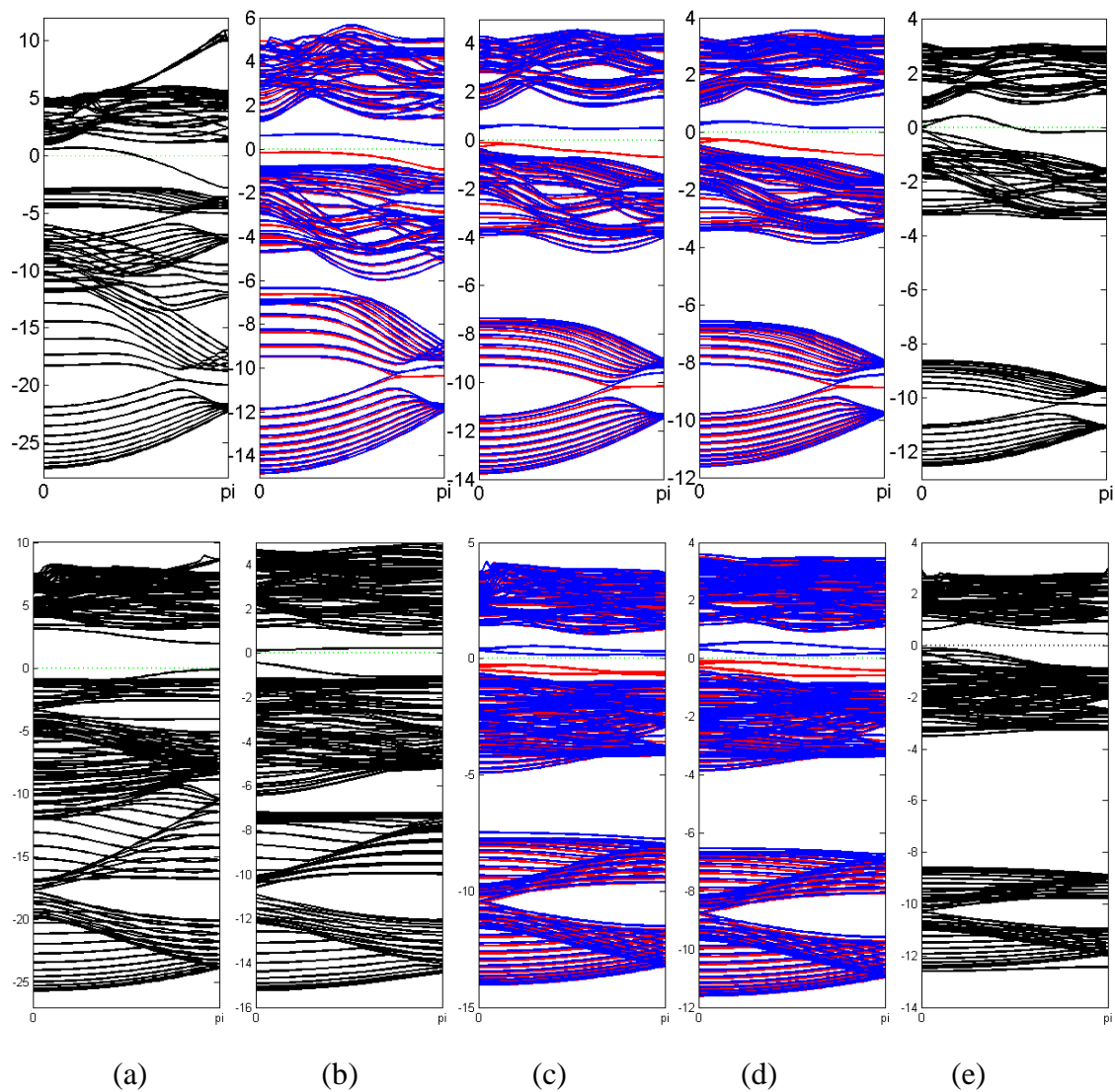


Figure 9 Band structure of ZNR (upper panel) and ANR (lower panel) for (a) nitrogen, (b) phosphorus, (c) arsenic, (d) antimony and (e) bismuth, respectively. The Fermi level is denoted by green dash line. For (b), (c) and (d), Red and blue solid lines refer to spin-up and spin-down, respectively.

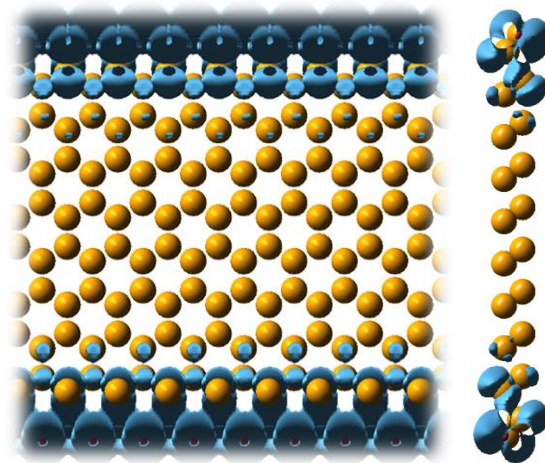


Figure 10 Charge density distribution of edge state in ZNR of P.

- 
- <sup>1</sup> Neto A. H. C. *et. al.* The electronic properties of graphene. *Rev. Mod. Phys.* **81**, 109 (2009)
  - <sup>2</sup> Wang Q. H. *et. al.* Graphene is not alone. *Nat. Nanotech.* **7**, 683 (2012)
  - <sup>3</sup> Splendiani A., *et. al.*, Emerging Photoluminescence in Monolayer MoS<sub>2</sub>, *Nano Lett.*, **10** (4), 1271 (2010)
  - <sup>4</sup> Wang Q. H., *et. al.* Electronics and optoelectronics of two-dimensional transition metal dichalcogenides, *Nature Nanotechnology*, **7**, 699–712 (2012)
  - <sup>5</sup> Novoselov K. *et. al.* Two-dimensional atomic crystals. *PNAS* **102**(30), 10451 (2005)
  - <sup>6</sup> Neto A. H. C. *et. al.* Two-Dimensional Crystals: Beyond Graphene. *Materials Express* **1**(1),10 (2011)
  - <sup>7</sup> Butler S. Z. *et. al.* *ACS nano* **7**(4), 2898 (2013)
  - <sup>8</sup> Castellanos-Gomez A. *et. al.* Isolation and characterization of few-layer black phosphorus. *2D Mater.* **1** 025001 (2014)
  - <sup>9</sup> Li L. K. *et. al.* Black phosphorus field-effect transistors. arXiv:1401.4117
  - <sup>10</sup> Liu H. *et. al.*, Phosphorene: A New 2D Material with High Carrier Mobility. *Nano Lett.* **8** (4) 4033 (2014)
  - <sup>11</sup> Zhu Z. and Tománek D., Semiconducting layered blue phosphorus: A computational study, *Phys. Rev. Lett.* **112**, 176802(2014)
  - <sup>12</sup> Guan J., *et. al.*, Phase Coexistence and Metal-Insulator Transition in Few-Layer Phosphorene: A Computational Study, *Phys. Rev. Lett.* **113**, 046804 (2014)
  - <sup>13</sup> Liu C. C., *et. al.*, Low-Energy Effective Hamiltonian for Giant-Gap Quantum Spin Hall Insulators in Honeycomb X-Hydride/Halide (X=N-Bi) Monolayers, *Phys. Rev. B* **90**, 085431 (2014)
  - <sup>14</sup> Song Z. G., *et. al.*, Quantum Spin Hall Insulators of BiX/SbX (X = H, F, Cl, and Br) Monolayers with a Record Bulk Band Gap, arXiv:1402.2399
  - <sup>15</sup> Chuang F. C. *et. al.*, Tunable topological electronic structures in Sb(111) bilayers: A first-principle study, *Appl. Phys. Lett.* **102**, 022424 (2013)
  - <sup>16</sup> Huang Z. Q. *et. al.*, Nontrivial topological electronic structures in a single Bi(111) bilayer on different substrates: A first-principle study. *Phys. Rev. B* **88**, 165301 (2013)
  - <sup>17</sup> Wang Z. F., *et. al.*, Tuning Topological Edge States of Bi(111) Bilayer Film by Edge Adsorption, *Nano Lett.* **14**, 2879 (2014)
  - <sup>18</sup> Yukihiro Harada *et. al.* Epitaxial two-dimensional nitrogen atomic sheet in GaAs. *Appl. Phys. Lett.* **104**, 041907 (2014)
  - <sup>19</sup> Andres C. G. *et. al.* Isolation and characterization of few-layer black phosphorus, *2D Mater.* **1** 025001 (2014)
  - <sup>20</sup> Cahangirov S., Topsakal M., Aktürk E., Şahin H., and Ciraci S., Two- and One-Dimensional Honeycomb Structures of Silicon and Germanium. *Phys. Rev. Lett.* **102**, 236804 (2009)
  - <sup>21</sup> Zdyomyi V., Wallbank J. R., Fal'ko V. I., Silicene and germanene: tight-binding and first-principles studies. *2D Mater.* **1** 011005 (2014)
  - <sup>22</sup> Liu C. C., Jiang H., and Yao Y. G. Low-energy effective Hamiltonian involving spin-orbit coupling in silicene and two-dimensional germanium and tin. *Phys. Rev. B* **84**, 195430 (2011)
  - <sup>23</sup> Yang F., *et. al.*, Time-Reversal-Invariant Topological Superconductivity in n-type Doped BiH, arXiv:1406.7316
  - <sup>24</sup> Okada S. and Oshiyama A., Magnetic Ordering in Hexagonally Bonded Sheets with First-Row Elements. *Phys. Rev. Lett.*, **87**, 146803 (2001)
  - <sup>25</sup> Bhowmick S. and Shenoy V. B. Edge state magnetism of single layer graphene nanostructures. *J. Chem. Phys.*, **128**, 244717 (2008)
  - <sup>26</sup> Perdew J. P., Burke K., and Ernzerhof M. Generalized Gradient Approximation Made Simple. *Phys. Rev. Lett.* **77**, 3865 (1996)
  - <sup>27</sup> Kresse G. and Furthmüller J., Efficient iterative schemes for *ab initio* total-energy calculations using a plane-wave basis set. *Phys. Rev. B* **54**, 11169 (1996)
  - <sup>28</sup> Grimme S. Semiempirical GGA-type density functional constructed with a long-range dispersion correction. *J. Comp. Chem* **27**, 1787 (2006)
  - <sup>29</sup> Klimeš J., Bowler D. R., and Michaelides A. Van der Waals density functionals applied to solids. *Phys. Rev. B* **83**, 195131(2011)
  - <sup>30</sup> [http://en.wikipedia.org/wiki/Periodic\\_table](http://en.wikipedia.org/wiki/Periodic_table)